

Design and Modeling of a Clutch Actuator System With Self-Energizing Mechanism

Jinsung Kim, *Student Member, IEEE*, and Seibum B. Choi, *Member, IEEE*

Abstract—The engineering technology for automotive systems is currently edging toward improving fuel economy. Transmission is one of the major parts to determine overall energy efficiency. The goal of this paper is to investigate the feasibility of a new clutch actuator in order to increase power transmitting efficiency. The new clutch actuator has self-energizing mechanism to amplify the normal force applied on the contact surfaces for the engagement. It allows the clutch module to consume less amount of energy for actuating the overall system. The equations of motion of the clutch mechanism coupled with a dc motor are represented to capture the essential dynamics. By using the proposed model, a model-based position-tracking controller is developed for the engagement of the clutch. Also, passivity analysis of the actuator system is performed to prevent the clutch from being stuck. Finally, the self-energizing effect and torque transmissibility of the proposed system and motion controller are validated experimentally.

Index Terms—Automotive system, clutch actuator, motion control, passivity, powertrain system, self-energizing effect.

I. INTRODUCTION

IN MANY engineering fields, newly designed actuators using novel drive principle, in conjunction with the advances in mechatronic technologies, have been researched and developed to improve conventional systems, i.e., an electromagnetic actuator [1], [2], dual actuator for interaction between force and position control [3], a rotary-linear actuator using piezoelectric translators [4], and a brushless dc motor integrating gear reducer [5], etc. They are considered in terms of integrating system design in aspect of control performance as well as the mechanical design aspect. Such approaches described earlier are also taken into consideration to automotive subsystems. Among many vehicle components, the transmission, which is one of the drivetrain components play a crucial role in determining the fuel efficiency of a vehicle.

In recent years, several types of automatic transmissions (ATs) have been developed besides traditional planetary type AT. Automated manual transmissions (AMTs) attract the driver's attention particularly in Europe. It is mostly the same as manual transmissions (MTs) except for some features. Compared with

MTs, the major difference is that the clutch actuator and synchronizers used in a gearbox for a gearshift are servoactuated hydraulically or electromechanically. The major drawback of AMTs is torque interruption while performing gearshift automatically. As a result, shift comfort or driver ability is degraded undesirably. It is thus required to develop a sophisticated control method for clutch engagement and synchronizers in order to preserve the passengers, comfort [6], [7].

In the early 2000, BorgWarner, an automotive transmission manufacturer in the U.S., has released a new type of AT, the so-called "dual clutch transmission (DCT)". DCTs take advantage of two separated power flows in order to transmit the torque generated from the engine. Unlike AMTs, there is a substantial incentive of reducing torque interruption during a gearshift. It should be noted that this characteristic allows DCTs to achieve good-shift comfort and improved fuel efficiency at the same time. DCTs are currently the most efficient automatics with up to 15% fuel efficiency improvement compared to planetary ATs. Moreover, fuel efficiency is improved even further up to 1.5% [8] with the use of dry clutches. In addition to this, the best performance could be also expected in conjunction with electromechanical actuations [9].

In terms of convenience and performance, DCTs and AMTs are expected to become standard types in the automotive transmission industry. Unfortunately, the conventional clutch systems with dry clutches used in transmissions are generally suitable for manual operation by a driver rather than automated controls [10]. Otherwise, they have been developed in a form of planetary AT especially with a wet clutch type. Moreover, hydraulic actuation devices have a significant proportion of the energy loss in transmission systems, although they are broadly used in transmissions and there are many advantages, such as force multiplication, compactness, and lubrication [11], [12]. Because of this, electromechanical technology is preferred as an alternative solution in terms of functionality and improved packaging [13], [14].

Thus, the development of a new actuator structure driven by an electromechanical device with a dry clutch is required to achieve the ultimate goal of maximizing fuel efficiency. Consequently, the objective of this paper is to design an alternative electromechanical clutch actuator system with a novel design concept that is suitable for servoactuation including dry-friction disks without large and expensive electric actuators. Self-energizing mechanism can be employed to reduce driving torque [15]. The similar approaches using ball-ramp mechanism are fine for ON/OFF-type control, but are not ideal for proportional torque control, since they suffer from instability problem of force control caused by ball stick and slippage [16], [17]. The

Manuscript received April 20, 2010; revised June 23, 2010; accepted June 25, 2010. Date of publication August 19, 2010; date of current version August 30, 2011. Recommended by Technical Editor J. M. Berg.

The authors are with the Department of Mechanical Engineering, Korea Advanced Institute of Science and Technology, Daejeon 305-701, Korea (e-mail: jsk@kaist.ac.kr; sbchoi@kaist.ac.kr).

Color versions of one or more of the figures in this paper are available online at <http://ieeexplore.ieee.org>.

Digital Object Identifier 10.1109/TMECH.2010.2059034

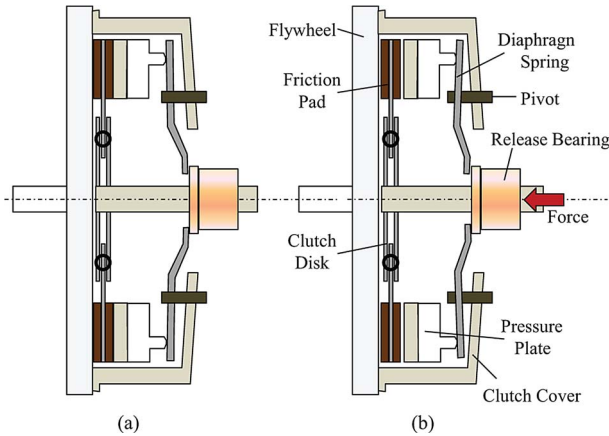


Fig. 1. Side view of conventional dry-clutch assembly. (a) Normally engaged phase. (b) Disengaged phase.

torque amplification of the ball-ramp actuators are typically in the range of 1:100. Also, each ball-ramp position is arbitrarily movable due to slip. Consequently, it is extremely difficult to control the torque proportionally.

In this paper, the clutch actuator system with rack and pinion mechanism as wedge mechanism is proposed to provide reinforcement of engagement force by self-energizing effect without slip and excessive force amplification to solve the problem described earlier.

This paper is organized as follows. In Section II, the design of an efficient clutch actuator incorporating self-energizing structure comparable to conventional clutch systems with a dry-friction disk is proposed. In Section III, the modeling of a mechanical clutch actuator is suggested to address the essential dynamics, which will be used for control design and system analysis. Section IV presents passivity analysis of the mechanical actuator system to avoid it being stuck resulting from excessive force amplification by virtue of self-energizing effect. In addition, a feedback controller is designed to control the motion of the actuator for clutch engagement. In Section V, experimental results are illustrated to validate and evaluate the torque transmissibility and the engagement performance. Section VI summarizes the conclusions and future works for this research.

II. DESIGN OF NEW CLUTCH ACTUATOR SYSTEM

A. Conventional Clutch System

The conventional dry-clutch actuator system has been broadly used in MT and AMT until now. It consists of clutch covers, a friction disk, a pressure plate, and a release bearing. Fig. 1 shows the schematic of a conventional dry-clutch assembly.

Dry-clutch components include a torsional damper, which plays a role of filtering out engine acyclicity with flywheel mass, which functions as an energy-storage element. Since this system is built in MT systems, the default position of dry clutch is normally closed forced by a diaphragm spring, which is at rest being compressed to around 400 N for a 200 mm clutch designed for mid-size cars [18]. Its working frequency is sensibly higher than the one involved in driveline oscillation. Therefore,

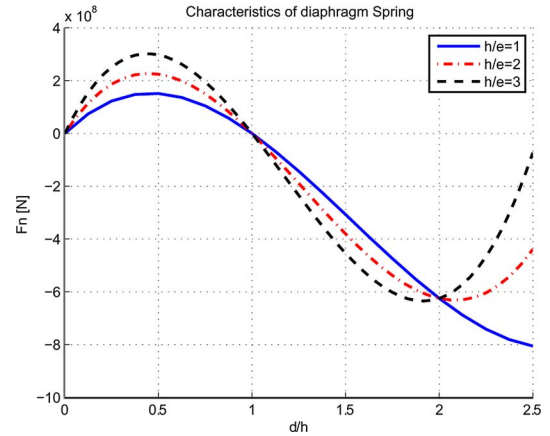


Fig. 2. Characteristic curves of diaphragm springs.

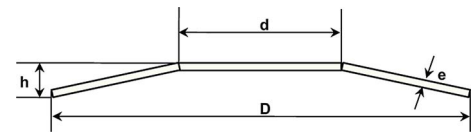


Fig. 3. Diaphragm spring structure (Belville spring).

the driveline oscillation can be triggered. General clutch operating force could be determined by the stiffness of a diaphragm spring. Figs. 2 and 3 show a diaphragm spring so-called Belville spring and its structure. The estimated force from its geometric condition can be calculated from

$$F_n = \frac{4EC}{1-\nu^2} \frac{e\delta}{D^2} \left((h-\delta) \left(h - \frac{\delta}{2} + e^2 \right) \right) \quad (1)$$

where $C = \pi(D/(D-d))^2((D+d)/(D-d) - 2)/(\ln(D/d))$, D is the external diameter of Belville spring, d is internal diameter, E is elastic modulus of given material, e is the thickness, h is the height of the spring, which is bent down, δ is the axial deformation with respect to applied force, and ν is the Poisson ratio of given material [19]. The characteristic curves of a diaphragm spring shown in Fig. 2 is calculated from (1). The ratio δ/h determines the characteristics of a diaphragm spring, and the normal force is a nonlinear function of spring deflection. In addition to the deflection ratio, the geometric constraint represented by h/e can also influence the characteristics. As illustrated in Fig. 2, the negative gradient of normal force allows a driver to reduce the effort for operating a clutch. The key advantage is that high load can be obtained by relatively small deflection of washer springs. They use the reaction of a diaphragm spring hinged to a pressure plate inside of a clutch cover, as shown in Fig. 1, but this characteristic imposes some limitations as follows.

- 1) First, nonlinear characteristic of a diaphragm spring is optimized with respect to driver's foot operations throughout a clutch pedal, may lead to degradation of control performance in automatics.
- 2) Second, since the system is operating under the normally engaged state, the preload δ on the diaphragm spring is needed to hold the engagement. However, it causes the

actuation force to be increased detrimentally in the automatics.

- 3) Third, the connecting element between the clutch plates and the actuator needs to be as stiff as possible to minimize the actuation energy loss for any level of required actuation force.

Under the circumstance, the operation of a clutch and gearbox actuators becomes automated using a transmission control unit linked to an engine control unit by virtue of the advances in electrical and electronic technology. Furthermore, high-torque transmissibility of an existing clutch actuator is required to meet the tendency of increasing engine torque in the automotive industry. Some of these problems give a motivation to design a new clutch actuator system without resorting to the use of a diaphragm spring especially for an automatic control system.

B. Design Concept: Self-Energizing Effect

A novel actuation strategy is suggested for the aforementioned reasons described in the preceding section. The key idea of a new clutch actuator design is the use of rack and pinion mechanism. This analogy is similar to an electronic wedge brake (EWB) system, which also includes wedge mechanism to reinforce actuation force [20]. Similar self-energizing effect can also be utilized in this clutch system.

Self-energizing action is the case that the friction-generated moment assists the applied force/torque without any cost, such as speed conversion having specific ratio [21], [22]. For example, a gear mechanism can increase in torque using various gear ratios, while reducing the speed ratio by the same amount. Here, the speed reduction can be considered as a cost for increasing torque in the process. Belt and lever mechanisms are also based upon the same principle. These are not self-energizing effect.

It should be noted that self-locking is a special case of self-energizing effect. The major difference between them is that whether the clutch is releasable or not. If the friction-generated moment to assists the actuation has reduced magnitude of the required actuating force/torque to a small value, it is considered as self-energizing effect. On the other hand, if self-locking occurs due to infinite gain, the clutch system stays locked with no external actuating torque [21]. The ball-ramp actuators mentioned in the previous section only give self-locking with infinite gain. Therefore, the releasable-locking condition is very important for the proposed system. Implementation of this characteristic to the clutch application will be discussed later.

C. Physical Design Description

Fig. 4 and Table I show the schematic structure of the clutch actuator system and the name of each part developed in this study. As mentioned earlier, an improved actuation strategy is needed to reduce the actuator size and overcome structural limitations. In order to apply wedge mechanism on a rotating disk for amplifying actuation force, traditional bevel gears are employed.

The teeth of the bevel gear are meshed with those of the inclined surface engraved in between an actuation plate and a fixed plate, as shown in Fig. 5. The tangential surfaces of the

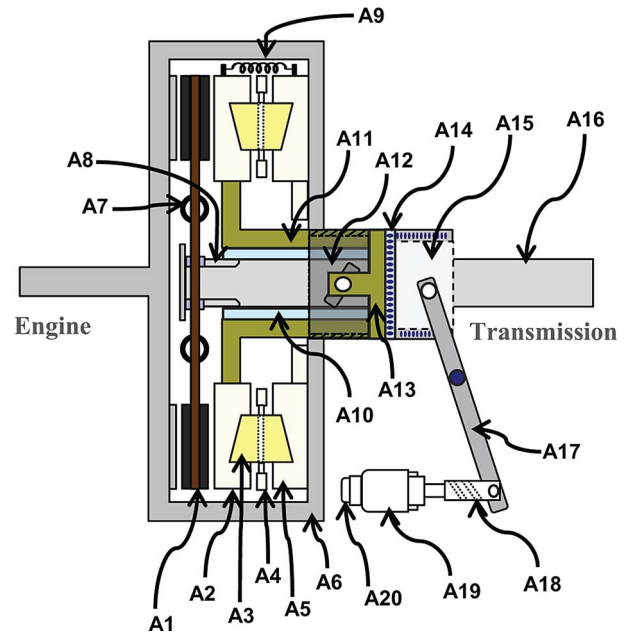


Fig. 4. Clutch actuator mechanism using self-energizing effect.

TABLE I
DESCRIPTION OF CLUTCH ACTUATOR PARTS

No.	Name	No.	Name
A1	Friction disk	A11	Actuation neck
A2	Actuation plate (Rack1)	A12	Worm shaft
A3	Pinion gear	A13	Slot joint
A4	Pinion guide	A14	Thrust bearing
A5	Fixed plate (Rack2)	A15	Thruster
A6	Clutch cover	A16	Transmission Input shaft
A7	Damper Spring	A17	Lever
A8	Spline	A18	Ball screw
A9	Return spring	A19	Electric motor
A10	Bearing	A20	Encoder

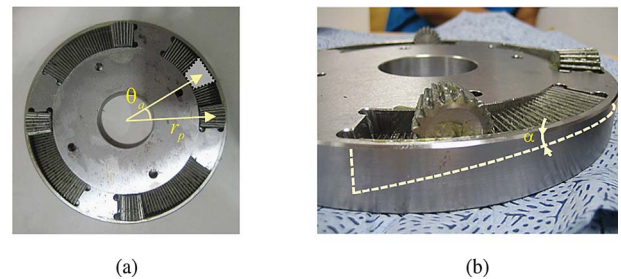


Fig. 5. Kinematic relation of the pinion gear and the plate. (a) Top view. (b) Side view.

pinions could physically keep in contact with teeth of the upper and lower racks if two supporting plates are constrained to be connected with each other by the clutch structure and return springs. It should be noted that three or more pinion gears are required to support both plates in parallel. The pinion gears are circumferentially in contact with the teeth of racks, as shown in Fig. 6. These are implemented not only for power reinforcement, but also for power transmission.

Then, the design of a structure for the delivery of the actuation force from an external electric motor to a mechanical structure

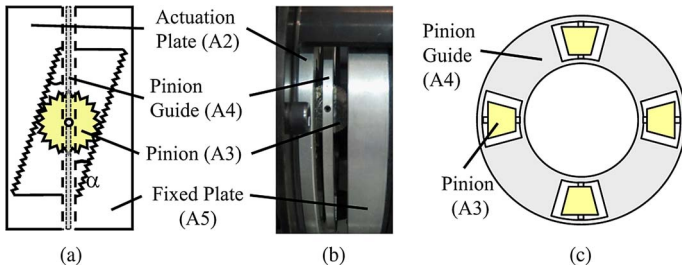


Fig. 6. Rack and pinion mechanism. (a) and (b) Side view. (c) Top view.

is another challenge at this stage. Some bearings are used to solve this problem. Based on Fig. 4, the release bearing has a sliding sleeve, which allows a radially inner sliding surface to be separated from the outer ring. The thrust bearing makes the applied force to be transferred to the actuation plate in axial direction. Also, the slot joint is employed for converting linear motion to rotational motion. Note that the design of parts except for rack and pinion mechanism would be improved with reduced weight and dimension for mass production.

D. Operation Principle

Referring to Figs. 4 and 7, an operation process for the clutch engagement is described in order. Once the electric motor (A19) is operated by a certain amount of current, 1) the ball screw (A18) and the lever (A17) transmit the torque to the thruster (A15). 2) The force is applied on the thrust bearing (A14). 3) The slot joint (A13) can move axially and rotate relative to the transmission input shaft by the bearing (A10). Also, it is connected with the actuation neck (A11) inside the worm shaft (A12). On the other hand, the worm shaft (A12) can neither move axially nor rotate because it is rigidly connected with the clutch cover. Since the slot joint (A13) and the actuation plate (A2) are connected in series via the actuation neck (A11), the actuation plate is rotated as the slot joint slides along the inclined groove. Then, 4) the rotational motion of the actuation plates coincides with the axial motion, since the pinions are formed on a circumference of the fixed plate having a certain radius from a center, thereof, on a surface inclined. Accordingly, by the axial motion of the actuation plate, 5) the friction disk, which is spline-connected in the transmission input shaft (A16), is forced toward the engagement position at which it contacts the opposite surface of the flywheel in the engine side. As a result, the nominal clutch torque is generated from frictional contact operation, and the self-energizing torque can also be generated from the inclined surface of the rack and pinion mechanism. In addition, it should be noted that the connection of the return springs (A9) between the fixed plate and the actuation plate should be needed to make the actuation plate return to a default position when the clutch is disengaged. Kinematic analysis of this operation is given in Appendix A.

E. Advantages

From the characteristics of the proposed system introduced in this section, the following advantages are expected.

- 1) Compared with ball-ramp mechanism, exploiting rack and pinion mechanism makes the contact operation more stable. Since the contact occurs along the line of action in rack and pinion mechanism, this basic characteristic of the gear train can guarantee smooth transition under the assumption that the geometric conditions of mechanism are well defined.
- 2) A diaphragm spring is eliminated. Thus, negative effects, such as nonlinearities and the preloading are also eliminated.
- 3) The required torque of the motor can be reduced significantly. It is enough to use standard 12 V vehicle electricity. It gives a substantial opportunity to develop a new actuation system that reduces a cost of a drivetrain system significantly.
- 4) It is possible to provide a one-way clutch characteristic, which is useful for preventing DCT systems from an undesirable situation like both clutches being engaged simultaneously.

III. DYNAMIC MODELS

In this section, the dynamic models for the clutch actuator with self-energizing effect are discussed to describe the motion of physical systems. The overall system can be divided into two parts, which are mechanically linked each other: an electric motor and a mechanical subsystem including a clutch disk. It will be used to design a controller to track the desired position and generate clutch torque on the friction surface for an engagement operation.

As a first step of modeling this system, a dc motor is considered to operate the mechanical clutch actuator. The motor electric and mechanical equations are as follows, respectively:

$$L_m \frac{di_m}{dt} + R_m i_m + V_{\text{emf}} = V_s \quad (2)$$

$$J_m \frac{d\omega_m}{dt} + T_{\text{fm}}(\omega_m) + T_L = T_m \quad (3)$$

In (2), V_s is the voltage applied to the motor, i_m is the motor current, R_m is the resistance, L_m is the inductance, and V_{emf} is the back electromotive force. In (3), J_m is the motor moment of inertia, ω_m is the rotor speed, T_m is the motor torque, T_{fm} is the nonlinear motor friction torque, and T_L is the load torque. The motor torque T_m is proportional to the current with the torque constant k_t as follows:

$$T_m = k_t i_m \quad (4)$$

The motor friction model is described as the static Coulomb and viscous friction map given by

$$T_{\text{fm}}(\omega_m) = \begin{cases} T_{\text{cm}+} + b_m + \omega_m, & \omega_m > \varepsilon_m \\ T_{\text{cm}-} + b_m - \omega_m, & \omega_m < -\varepsilon_m \\ T_m, & \text{if } |\omega_m| < \varepsilon_m \text{ and } |T_{\text{fm}}| < T_{\text{fsm}} \\ T_{\text{fm}} \text{sgn}(T_m), & \text{if } |\omega_m| < \varepsilon_m \text{ and } |T_{\text{fm}}| > T_{\text{fsm}} \end{cases} \quad (5)$$

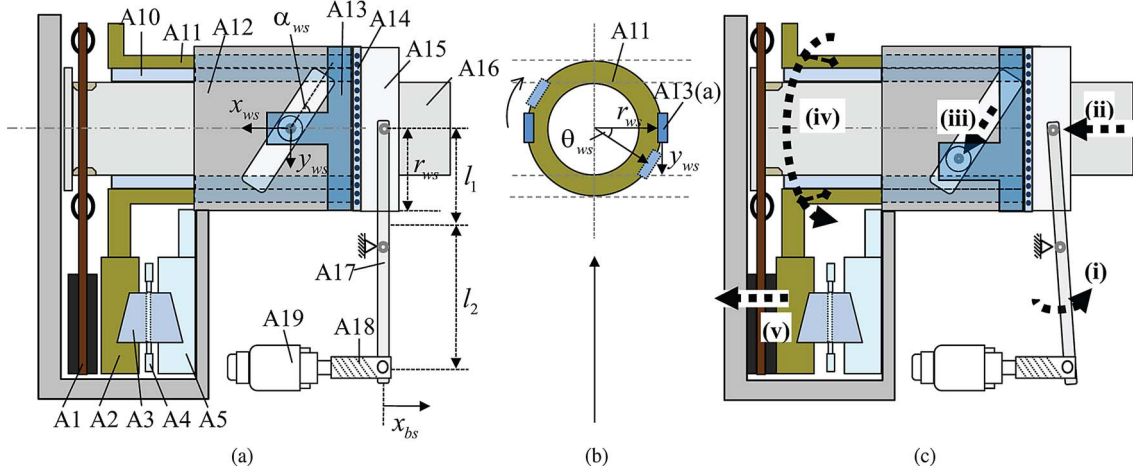


Fig. 7. Operation principle of the clutch actuator system (detailed descriptions are given in Section II-D and Appendix A). (a) Disengaged phase. (b) Cross section of the worm shaft observed on the left side of (a). (c) Engaged phase.

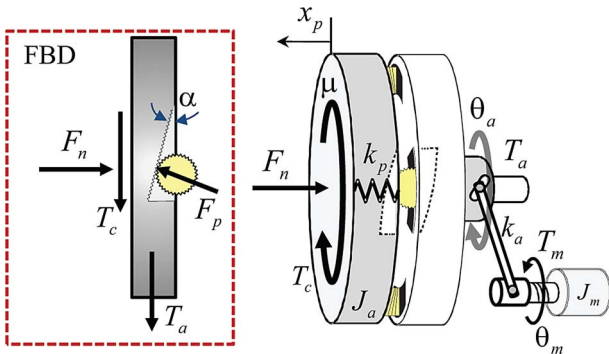


Fig. 8. Schematic of the equivalent clutch actuator model.

where T_{cm} is the motor Coulomb friction torque, b_m is the motor viscous friction coefficient, and T_{fsm} is the motor static-friction torque. The friction model described earlier is based on the Karnopp approach to solve the chattering problem between sticking and sliding in the vicinity of zero velocity [23]. ε_m denotes a small zero velocity interval in which the velocity of the motor is considered as zero. The subscripts “+” and “-” are used to represent the hysteresis phenomenon.

The fixed plate (A5 in Fig. 4) shown in Fig. 8 is interposed between the clutch cover and the friction disks in order to adjust the axial displacement of the actuation plate (A2 in Fig. 4), while rotating at the same time. In free space, the rotational equation of motion for the actuation plate without the clutch engagement torque is described as follows:

$$J_a \dot{\omega}_a = T_a - T_{fa}(\omega_a) \quad (6)$$

where J_a is the moment of inertia of the actuation plate. Since the pinions are constrained by two supporting plates (A2 and A5 in Fig. 4) and the pinion guide (A4 in Fig. 4), the motion of them coincides with the actuation plate. Thus, it is reasonable to assume that the inertia of the pinions is lumped into that of the actuation plate. Note that this constrained structure is advantageous to obstruct backlash of the pinion gear during operation. In the (6), the frictional torque T_{fa} on the worm shaft

is represented by the following static-Coulomb-viscous friction model:

$$T_{fa}(\omega_a) = \begin{cases} T_{ca+} + b_a \omega_a, & \omega_a > \varepsilon_a \\ T_{ca-} + b_a \omega_a, & \omega_a < -\varepsilon_a \\ T_a, & \text{if } |\omega_a| < \varepsilon_a \text{ and } |T_{fa}| < T_{fsa} \\ T_{fs} \text{sgn}(T_a), & \text{if } |\omega_a| < \varepsilon_a \text{ and } |T_{fa}| > T_{fsa} \end{cases} \quad (7)$$

where T_{ca} is the actuator Coulomb friction torque, b_a is the actuator viscous friction coefficient, and T_{fsa} is the actuator static-friction torque. ε_a denotes a small zero velocity interval in which the velocity of the actuator is considered as zero. Note that the subscripts “+” and “-” are also used to represent the hysteresis phenomenon. The equivalent torsional stiffness k_a of the mechanical link between the lever and the worm shaft can be represented as a series of the torsional stiffness of the ball screw k_{bs} and the lever k_l [24]

$$k_a = \left(\frac{1}{k_{bs}} + \frac{1}{k_l} \right)^{-1}. \quad (8)$$

Then, the driving torque T_a is transferred from the motor to the mechanical actuator due to an elastic deformation with the equivalent torsional stiffness k_a as follows:

$$T_a = k_a \left(\frac{\theta_m}{N_g} - \theta_a \right) \quad (9)$$

where θ_a is the actuator angular position, and N_g is the equivalent conversion ratio between the motor and the actuator angular position. Further details for the derivation of N_g is given in Appendix A. Since the load torque T_L in the motor dynamics (3) is the driving torque T_a introduced in (6) and (9), the following relationship is satisfied, i.e., $T_L = T_a/N_g$.

When the clutch is in contact with the surface for engagement operation, the clutch torque and the reinforcement torque is added in (6), as shown in Fig. 8. Therefore, the equation of motion for the actuation plate in the slip phase is represented by

$$J_a \dot{\omega}_a = T_a + T_c - 2r_p F_p \sin \alpha - T_{fa}(\omega_a) \quad (10)$$

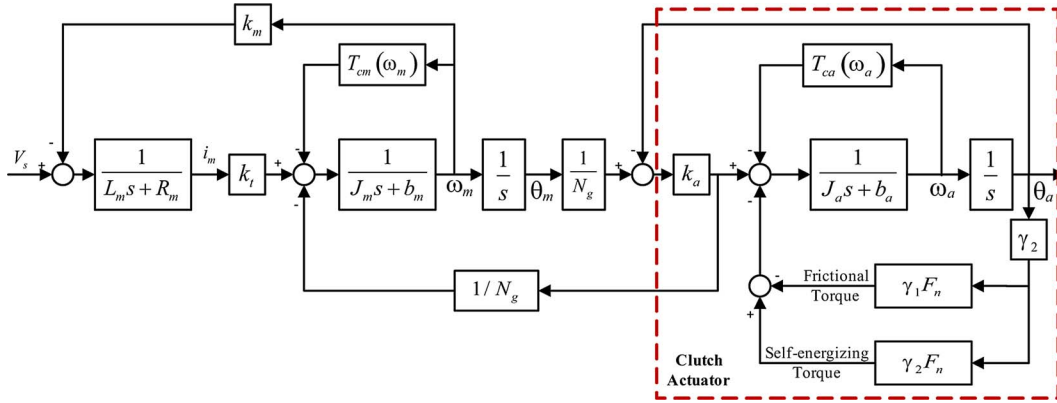


Fig. 9. Block diagram of the system model in the slip phase.

where T_c is the clutch torque, F_p is the reaction force on the rack and pinion surface, and r_p and α are the radius of bevel gear position and the inclined surface angle on the actuation plate and the fixed plate, respectively. By the assumption of the positive-slip phase, the clutch torque T_c is obtained as follows:

$$T_c = \mu R_c F_n \quad (11)$$

where μ is the dry-friction coefficient, R_c is the clutch radius, and F_n is the applied normal force. Since there is rack and pinion mechanism, the relationship between F_p and F_n is determined by the inclined surface angle α , as shown in Fig. 8. As a result, F_p is given as follows:

$$F_p = \frac{F_n}{\cos \alpha}. \quad (12)$$

Note that the third term at the right-hand side in (10) is related to self-energizing effect. The existence of rack and pinion mechanism can induce the reaction force F_p on the surface of the actuation plate and the fixed plate with respect to the applied normal force F_n .

The axial displacement of the actuation plate can be calculated through the geometric relation, as shown in Fig. 5. It is, therefore, given by

$$x_p = 2r_p \theta_a \tan \alpha \quad (13)$$

where θ_a is the angular position of the actuation plate. The normal force applied on the friction disk is

$$F_n = k_p x_p = 2k_p r_p \theta_a \tan \alpha \quad (14)$$

where k_p is the stiffness of the actuation plate. It is assumed that the normal force F_n is proportional to the actuator stroke x_p in axial direction.

According to (12)–(14), then the actuator dynamics (10) in the positive-slip phase can be rewritten as follows:

$$J_a \dot{\omega}_a = T_a + F_n(\gamma_1 - \gamma_2) - T_{fa}(\omega_a) \quad (15)$$

where

$$\gamma_1 = \mu R_c$$

$$\gamma_2 = 2r_p \tan \alpha.$$

The block diagram of the overall system model is illustrated in Fig. 9 and the description for system model parameters are presented in Appendix B.

IV. SYSTEM ANALYSIS AND CONTROL DESIGN

A. Torque Amplification Effect

The key advantage of the proposed concept is the use of self-energizing effect. The inclined surface angle denoted by α is a very important parameter because it determines the magnitude of the amplification. Motivated by the clutch actuator model (15), the torque amplification ratio in this system can be simply formulated by the static function. The operating phase is assumed as a steady state in which the clutch is engaged and motion of the actuator remains thereafter. The torque amplification ratio Υ can be defined by the resulting clutch torque T_c to the actuator driving torque T_a as follows:

$$\Upsilon \triangleq \frac{T_c}{T_a} = \frac{\mu R_c}{2r_p \tan \alpha - \mu R_c} \approx \frac{\mu}{2 \tan \alpha - \mu}. \quad (16)$$

Unless the system has the rack and pinion mechanism ($\alpha = 0$), the third term at the right-hand side in (10) is eliminated. Therefore, the ratio in (16) becomes one. Then, the resulting clutch torque T_c is equal to the driving torque T_a under the assumption that disturbances, such as friction are neglected. It means that if the higher clutch torque capacity is required corresponding to the higher engine torque, large and expensive electric motors should be needed that also cause increased space requirements.

Also, the torque amplification ratio Υ may abruptly be large over a certain value of the friction coefficient. Moreover, when the friction coefficient μ is greater than $2 \tan \alpha$, relatively large normal force F_n is needed to ensure the engagement. Thus, it is apparent that the condition of $\mu < 2 \tan \alpha$ should be satisfied. This intuitive result can also be proved by the following analysis.

B. Passivity Analysis

The passive properties are commonly used to analysis and design of mechanical systems and originate in the notion of energy [25]–[27]. A system is said to be passive if the energy absorbed over any period of time is greater than or equal to the

increase in the energy stored over the same period [28], [29]. The observation of input and output energy pairs could give physical intuition of system characteristics. The proposed system should guarantee a releasable structure-locking connection in order to avoid getting stuck in uncontrolled-locking phase, although the reinforcement torque generated from a self-energizing structure makes the actuation energy be reduced significantly. Since the equations of motion in Section III show that the driving torque of the actuation plate T_a is proportional to the motor applied voltage V_s , the actuator driving torque T_a is considered as a system input for the analysis. Since the actuation plate has very high stiffness, it is reasonable to assume that the bandwidth of the actuator parts is much higher than that of the closed-loop system.

Assumption 1: γ_1 is uncertain and varies with several factors of dry friction, such as temperature, clutch wear, and material properties. Even though the actual value is unknown, it is limited between lower and upper bounds due to the physical nature of dry friction.

$$\gamma_1 \in \Gamma \triangleq \{\gamma_1 : \gamma_{1\min} \leq \gamma_1 \leq \gamma_{1\max}\}. \quad (17)$$

Assumption 2: The normal force F_n is a piecewise linear function of the actuator stroke x_p at least [6], [30].

Lemma 1 (In free space (clutch open)): The dynamical clutch actuator system is passive with supply rate $s(\omega_a, T_a) := \omega_a T_a$

Proof: Consider the following positive-definite Lyapunov function V yields

$$V = \frac{1}{2} J_a \omega_a^2. \quad (18)$$

Its time derivative is as follows:

$$\begin{aligned} \dot{V} &= J_a \omega_a \dot{\omega}_a = J_a \omega_a \left(\frac{T_a - T_{fa}(\omega_a)}{J_a} \right) \\ &= \omega_a T_a + \omega_a T_{fa}(\omega_a). \end{aligned} \quad (19)$$

The second term $\omega_a T_{fa}(\omega_a)$ in aforementioned equation is bounded and dissipative. Therefore,

$$\begin{aligned} V(t) - V(0) &= \int_0^t s(\omega_a, T_a) d\tau - \int_0^t \omega_a T_{fa}(\omega_a) d\tau \\ &\leq \int_0^t s(\omega_a, T_a) d\tau. \end{aligned} \quad (20)$$

This result clearly shows the actuator system is passive. ■

Once the clutch is engaged, the motion of the actuator is constrained with its stroke limit. In the engaged phase, the clutch torque is generated from interfacial contact with self-energizing torque depending on the geometric condition. When the clutch is engaged, the following lemma can be derived.

Lemma 2 (Releasable-locking condition): Let the actuator initial position be the kissing point $\theta_a(0) = 0$. Under Assumptions 1 and 2, the dynamical clutch actuator system (10) is passive with supply rate

$$s(\omega_a, T_a) := \omega_a T_a \quad (21)$$

when the clutch plates are in contact if the following condition is satisfied:

$$\left(1 - \frac{\gamma_{1\max}}{\gamma_2} \right) > 0. \quad (22)$$

Proof: Defining a Lyapunov function V satisfying positive-definite condition yields

$$V = \frac{1}{2} J_a \omega_a^2 + \frac{1}{2} k_p \left(1 - \frac{\gamma_{1\max}}{\gamma_2} \right) x_p^2. \quad (23)$$

Its time derivative is as follows:

$$\begin{aligned} \dot{V} &= J_a \omega_a \dot{\omega}_a + k_p \left(1 - \frac{\gamma_{1\max}}{\gamma_2} \right) x_p \dot{x}_p \\ &= \omega_a [T_a + \gamma_1 F_n - \gamma_2 F_n - T_{fa}] + k_p x_p \dot{x}_p - k_p x_p \frac{\gamma_{1\max}}{\gamma_2} \dot{x}_p. \end{aligned} \quad (24)$$

From (12), this can be rewritten as follows:

$$\begin{aligned} \dot{V} &= \omega_a [T_a + \gamma_1 F_n - \gamma_2 F_n - T_{fa}(\omega_a)] \\ &\quad + \omega_a \gamma_2 F_n - \omega_a \gamma_{1\max} F_n \\ &= \omega_a T_a - \omega_a T_{fa}(\omega_a) + \omega_a F_n (\gamma_1 - \gamma_{1\max}) \leq \omega_a T_a. \end{aligned} \quad (25)$$

In the last step in (25), the fact that $\gamma_1 - \gamma_{1\max} < 0$ is always satisfied is used. Since the supply rate is defined as (21), integration of the last term in aforementioned equation is rewritten as follows:

$$\int_0^t s(\omega_a, T_a) d\tau \geq V(t) - V(0). \quad (26)$$

This means that the power flow into the system is greater than or equal to the rate of change of the energy stored in the system by the condition (22). Thus, the proposed actuator system is passive. ■

Rotational motion of the actuator generates axial motion along the driving shaft at the same time due to the self-energizing structure.

Remark 1: The results show that the self-energizing torque implies a mechanical feedback of the frictional clutch torque T_c by combined motion of the actuator with passivity property. The Lemma 2 can provide a condition of the mechanical design and a guide to appropriate control action.

Remark 2: It is clear from (10) that γ_1 and γ_2 are mean frictional torque gain and self-energizing torque gain, respectively. The inequality (22) enables the Lyapunov function to be positive-definite function and gives a guide to determining design parameters. It is assumed that R_c is equal to r_p as geometrically on the clutch surface. Therefore, the condition (22) can be rewritten as follows:

$$\mu_{\max} < 2 \tan \alpha \quad (27)$$

where μ_{\max} is the maximum value of a dry-friction coefficient. The nominal range of dry-clutch friction coefficient is from 0.27 to 0.45 approximately. Fig. 10 shows the gain characteristics in terms of the inclined surface angle and the torque amplification

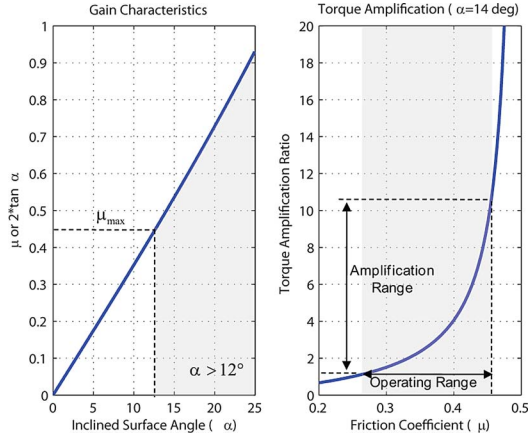


Fig. 10. Parameter design of the inclined surface angle. (Left) Gain characteristics. (Right) Torque amplification ratio.

ratio. In this study, 14° is determined from the result of the passivity analysis results.

C. Motion Control

1) *Simplified Model*: Model simplification is needed to design a model-based controller. Since the electrical dynamics is much faster than the mechanical motion, it is reasonable to neglect the inductance parameter in (2) [31]. In addition, the actuation plate dynamics (10) has very high bandwidth and its rotating angle is very small compared with the motor rotation. These characteristics ensure the linear characteristic between its stroke in axial direction and the resulting clutch torque. Thus, it is assumed that the mechanical actuator is rigidly coupled with the dc motor. As a result, the equations of motion (2), (3), and (10) are rewritten as follows.

1) Motor model:

$$J_m \dot{\omega}_m = \frac{k_t}{R_m} V_s - \left(\frac{k_t k_m}{R_m} + b_m \right) \omega_m - T_{fm}(\omega_m) - \frac{T_a}{N_g}. \quad (28)$$

2) Load torque model:

$$T_a = T_{fa}(\omega_a) - \gamma_1 F_n + \gamma_2 F_n. \quad (29)$$

Therefore, the desired actuator position to be controlled can be replaced it with the motor position.

2) *Sliding-Mode Control*: Since the diaphragm spring, which may induce nonlinearities is eliminated in this system, the clutch actuator system is accounted as a typical linear motion control system [32], [33]. Therefore, the clutch engagement control is replaced with the clutch actuator positioning problem. Since this study seeks to verify the design feasibility of a self-energizing clutch actuator, such consideration is very useful. The operating range of the clutch actuator is always above the idle speed of internal combustion engines. This means that clutch positioning in the actuator is carried out, while the clutch overall structure, rigidly connected with the engine flywheel, is rotating to avoid undesirable engine stall. Therefore, there

are some parametric uncertainties in the dynamic model, since the clutch positioning should be conducted while rotating. For instance, the static-friction model of the worm shaft described in (7) is very sensitive to the actuator rotating speed ω_a . Based on the model validation result, there is some nonlinear friction behavior on the worm shaft motion due to hysteresis effect (see Fig. 13). Moreover, the clutch torque and its self-energizing one, which is induced by the clutch engagement cause bounded disturbances to the actuator system. The model simplification in the preceding section may also lead to system parametric uncertainty and unmodeled dynamics. Thus, sliding-mode controller is designed to ensure the motor (or actuator) position tracking for validating engagement test of the proposed system. It is well known that this control methodology is robust to parametric uncertainties and external disturbances. In our application that will be introduced later, the discontinuous control function in ideal sliding-mode control is replaced with the continuous approximation to avoid the chattering effect. This methodology may degrade tracking performance at a steady state due to introducing a boundary layer. To solve this, integral action can be added to reduce steady-state error [31], [37]. Consequently, position-tracking performance will be guaranteed. Note that the control issue at this step only takes clutch positioning into account and whether the clutch with the proposed mechanism is engaged or not. Define the tracking error in terms of the motor angular position θ_m and its desired trajectory θ_{md} , i.e., $e_m = \theta_{md} - \theta_m$. The sliding surface z is represented using the tracking error e_m as follows:

$$z = \dot{e}_m + K_P e_m + K_I \int_0^t e_m d\tau \quad (30)$$

where K_P and K_I are design parameters for determining desired error dynamics. Combining with the system model equations, the time derivative of the sliding surface (30) can be represented as follows:

$$P_1 \dot{z} = P_1 (\ddot{\theta}_{md} + K_P \dot{e}_m + K_I e_m) + P_2 \omega_m + P_3 + P_4 - V_s \quad (31)$$

where $P_1 = J_m R_m / k_t$, $P_2 = R_m / k_t (k_t k_m / R_m + b_m + b_a / N_g^2)$, $P_3 = (R_m / k_t) T_{fm}(\omega_m) + (R_m / k_t N_g) T_{fna}(\omega_m / N_g)$, and $P_4 = (R_m / k_t N_g) F_n (\gamma_1 - \gamma_2)$.

Assumption 3: The actuator system has parametric uncertainties, but bounded values are known. The bounds are $P_1 \leq \bar{P}_1 \leq \underline{P}_1$, $P_2 \leq \bar{P}_2 \leq \underline{P}_2$, $P_3 \leq \bar{P}_3 \leq \underline{P}_3$, and $P_4 \leq \bar{P}_4 \leq \underline{P}_4$, where P and \bar{P} are lower and upper bounds, respectively.

The following control law is suggested to track the desired actuator motion trajectory:

$$V_s = K_v z + \bar{P}_1 (\ddot{\theta}_{md} + K_P \dot{e}_m + K_I e_m) + \bar{P}_2 \dot{\theta}_m \text{sgn}(\dot{\theta}_m z) + \bar{P}_3 \text{sgn}(z) + \bar{P}_4 \text{sgn}(z). \quad (32)$$

Proposition 1: In constrained motion, consider an actuator system (28) with Assumptions 1, 2, 3, and Lemma 2 and the desired trajectories θ_{md} , $\dot{\theta}_{md}$, and $\ddot{\theta}_{md}$. The control law (32) ensures that the filtered tracking error $z(t)$ converges to zero asymptotically.

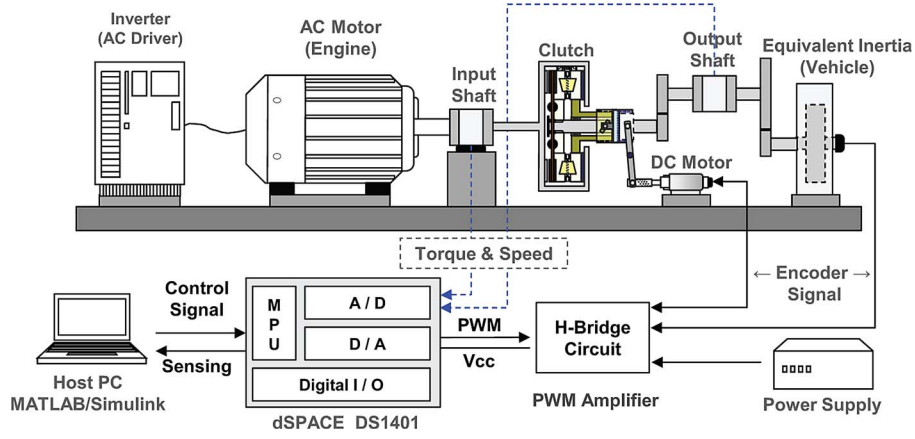


Fig. 11. Description of the experimental setup.

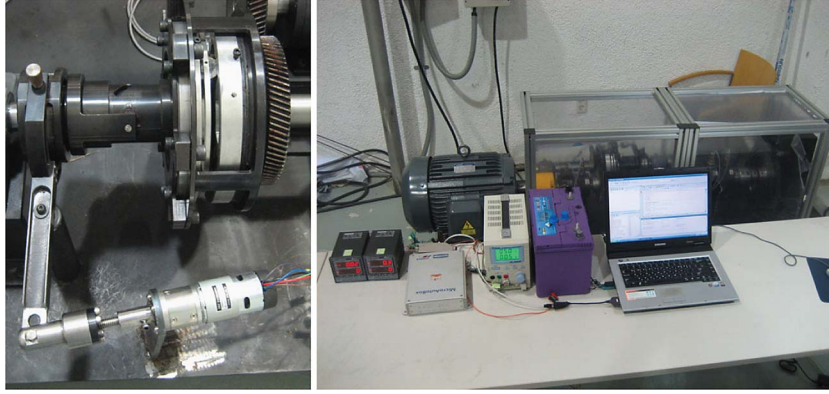


Fig. 12. Photograph of the experimental setup.

Proof: Define a positive-definite Lyapunov function V_c as follows:

$$V_c = \frac{1}{2} P_1 z^2 \quad (33)$$

The time derivative of (33) is as follows:

$$\begin{aligned} \dot{V}_c &= P_1 \dot{z}z \\ &= -K_v z^2 + P_1 |(\ddot{\theta}_{md} + K_P \dot{e}_m + K_I e_m)z| + P_2 |\dot{\theta}_m z| \\ &\quad + P_3 |z| + P_4 |z| - \bar{P}_1 |(\ddot{\theta}_{md} + K_P \dot{e}_m + K_I e_m)z| \\ &\quad - \bar{P}_2 |\dot{\theta}_m z| - \bar{P}_3 |z| - \bar{P}_4 |z| \leq -K_v z^2 < 0. \end{aligned} \quad (34)$$

This shows that the filtered tracking error $z(t)$ asymptotically converges to zero. ■

In practical environment, the signum function may lead to the chattering problem due to the measurement noise and some delay from the actuators. This can be eliminated by employing a saturation function with the boundary layer thickness Φ as the continuous approximation of a signum function [34], [35]

$$\text{sat}\left(\frac{z}{\Phi}\right) = \begin{cases} \frac{z}{\Phi}, & \text{if } \left|\frac{z}{\Phi}\right| < 1 \\ \text{sgn}\left(\frac{z}{\Phi}\right), & \text{otherwise.} \end{cases} \quad (35)$$

Thus, the signum functions in the control law (32) can be replaced by the saturation functions.

V. EXPERIMENTAL VERIFICATIONS

A. Experiment Setup

The laboratory test bed, in which torque transmissibility and actuator motion control experiments are performed, is set up. Fig. 11 shows the schematic diagram of experimental setup that consists of an ac motor, its inverter, a clutch assembly, a gear-box, and an equivalent inertia disk corresponding to the engine, clutch, transmission, and vehicle mass in automotive systems, respectively. The ac motor having a role of an automotive engine is controlled by the inverter. Two torque sensors including shaft speed measurement function are installed between the input and the output shafts of the clutch. The equivalent inertia disk, in which an additional optical encoder is attached, is used to describe the typical vehicle mass of a mid-size car.

The control system is implemented using a dSPACE Microautobox DS1401 board including a digital signal processor. This equipment is executed at a sampling frequency of 1 kHz. An electric actuator, which consists of a dc motor, a gear head, and a ball-screw combination controlled by a PWM servo amplifier, is designed to manipulate the lever (see Fig. 4). The required maximum torque range of 0 to 2 N·m, i.e., selected based on

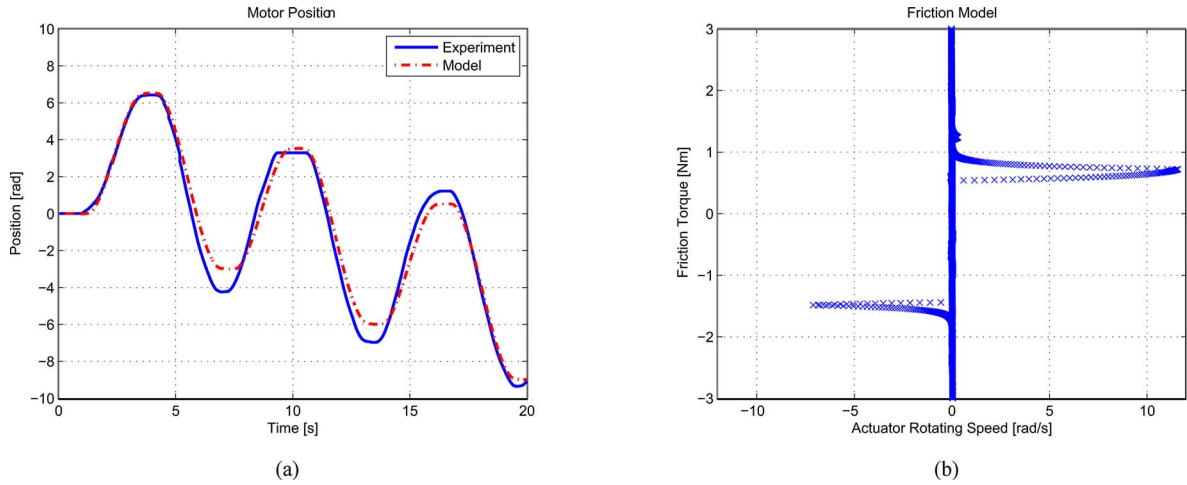


Fig. 13. System identification results. (a) Input voltage command test of the clutch actuator: 0.15 Hz sine wave input with 6 V peak-peak. (b) Friction characteristics of the clutch actuator worm shaft: 0.15 Hz sine wave input with 3 V peak-peak.

force measurement experiment using a load cell. A hall sensor is used to measure the motor angular position at the resolution of 145 pulse/rad resolution. The motor velocity signal is calculated from the difference between two consecutive position values at each sampling instant. The experimental devices are shown in Fig. 12.

B. Model Validation

To validate the developed model and design a controller, experimental identifications are performed by using the proposed prototype actuator. The nominal motor parameters are determined separately from any external load. Nonlinear least-square method is employed to identify the system parameters through pseudorandom binary noise signal excitation [36]. Then, the parameters for the clutch actuator part connected with the electric motor are obtained from a series of motion tests.

The model validation result is as illustrated in Fig. 13. The presence of friction on the worm shaft should be investigated to improve the modeling accuracy. Different amplitude voltage inputs are applied to the motor amplifier with a 0.15 Hz sine wave under an open-loop operation, as shown in Fig 13(a). Fig. 13(b) shows the friction phenomenon with hysteresis characteristics of the worm shaft. Multiple sets of data points have been measured for several repeated engagement tests using the torque transducer, as shown in Fig. 14. The interpolation curve is identified as a function of the clutch actuator stroke, i.e., $T_c = T_c(x_p)$.

C. Actuator Motion Control

Actuator control scheme developed in Section IV is verified within a free motion range, where the friction disk surface is not in contact with the other side. This test is conducted just to confirm the clutch positioning performance before the verification of the clutch engagement.

Fig. 15 depicts the experimental result of clutch actuator position control. The tracking response is good enough, although

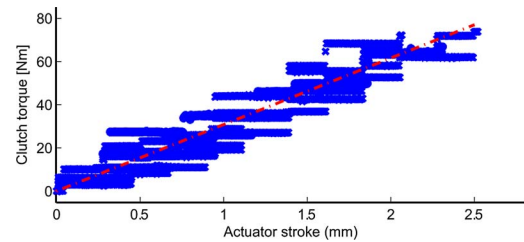


Fig. 14. Clutch torque characteristic. Experimental data (set of points) and torque characteristic curve (dashed-dotted).

there is some transient error right after the control action starts at 0.1 s due to the actuator saturation shown in Fig. 15(b).

D. Engagement Test

By using the position control strategy, the engagement control is conducted to validate whether the clutch torque is transmissible or not. The initial motor position is set 3 rad away from the opposite of the disk surface kissing point. The results of positioning control for the clutch engagement are illustrated in Fig. 16. In Fig. 16(a), the kissing point, where the clutch contact transition occurs is observed approximately at 5.2 s. Therefore, it is shown in Fig. 16(b) that some position errors appear as the clutch enters the slip region. Although there are some errors originated from the unexpected impact, the control action can overcome these disturbances. As a result, the tracking errors converge to zero in the steady state. In this paper, we restrict the test scope to launch operation, since the objective is the feasibility study of the proposed actuator. Considering gearshift operation makes the control system more challenging, since it is performed in a very short period of time.

E. Verification of Self-Energizing Effect

As shown in Fig. 14, the identified clutch torque includes the self-energizing torque as well as the nominal frictional torque.

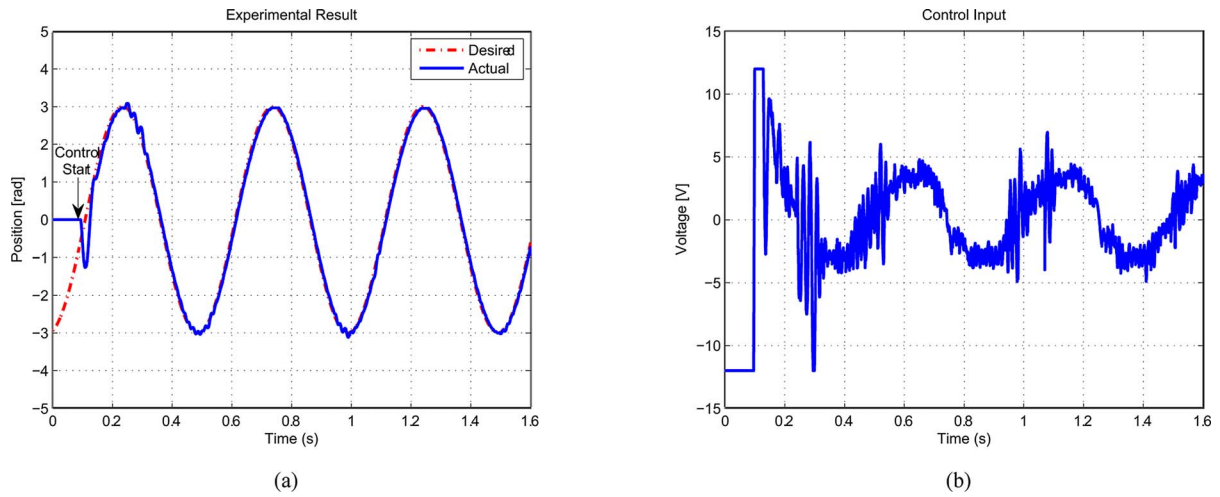


Fig. 15. Experimental results. Sliding-mode control for the clutch actuator motion. (a) Position tracking control. (b) Control input voltage.

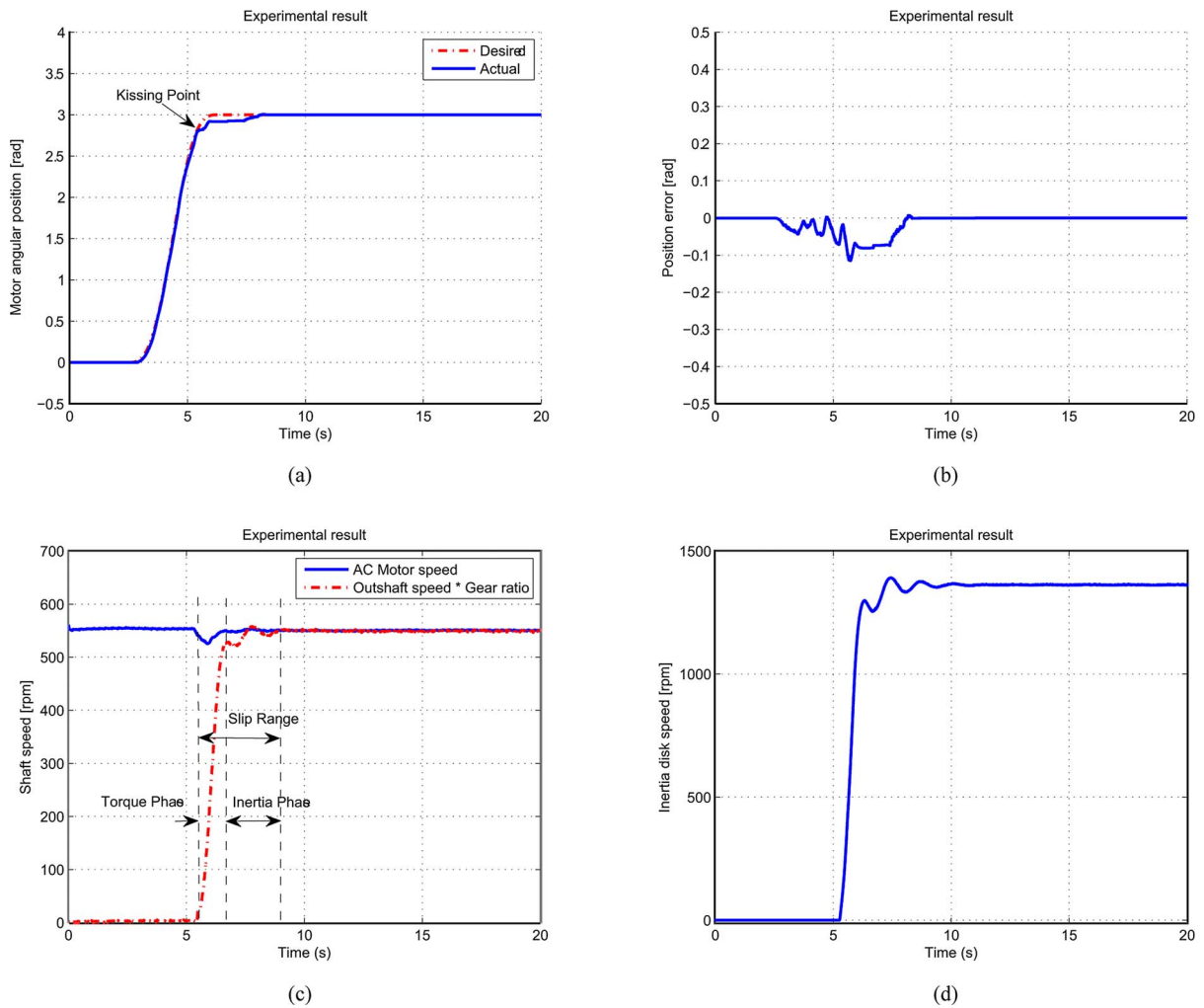


Fig. 16. Experimental results: clutch engagement test by actuator positioning control. (a) Clutch positioning result. (b) Motor position tracking error. (c) Input and output shaft speed. (d) Equivalent inertia disk speed.

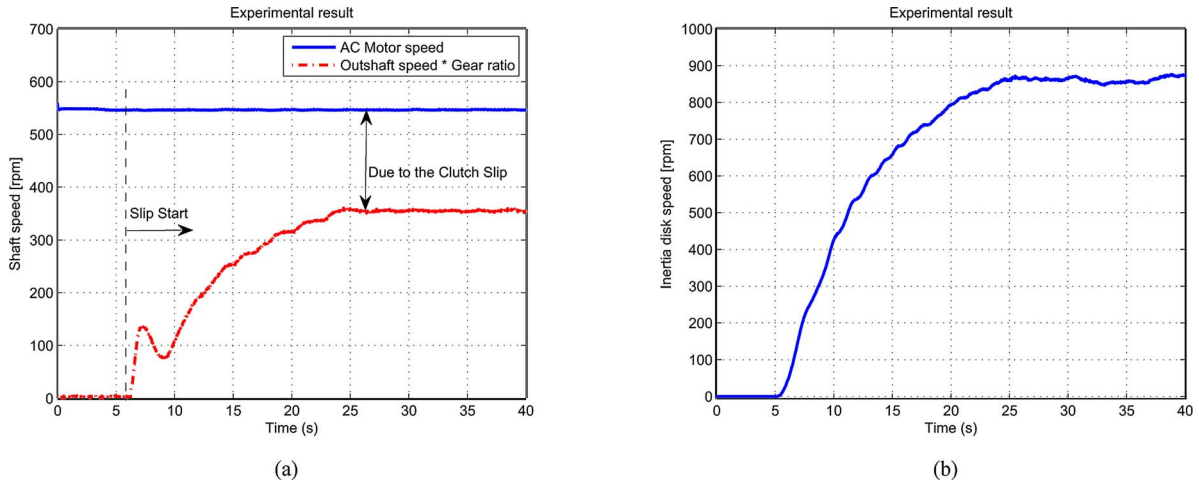


Fig. 17. Experimental results: reverse rotating test for verifying self-deenergizing effect. (a) Input and output shaft speed. (b) Equivalent inertia disk speed.

TABLE II
PERFORMANCE OF ENGAGEMENT TESTS

Case	$\max P [W]$
Self-energizing	1460
Self de-energizing	297.5

To verify the self-energizing effect, another experimental test is performed with the ac motor rotating in reverse. The result of this test is depicted in Fig. 17. From 6 to 10 s in Fig. 17(a), the negative gradient of the clutch output shaft speed is observed. It is apparent that the excessive slip occurs due to insufficient engagement torque from self-deenergizing effect. Comparing Fig. 17(a) and Fig. 15 (c), the major difference is that both sides of clutch are not synchronized although the clutch normal force is exerted on the friction disk by the motor actuation. The slip range is kept for a long period of time after the clutch comes into contact. It is clearly seen that the self-deenergizing case consumes a large amount of energy compared with the self-energizing case.

In particular, Table II shows maximum power during the engagement as a performance index. In the self-energizing case, maximum power is larger than in the self-deenergizing case. As a result, the advantage of using self-energizing mechanism is validated. In addition to this, self-deenergizing effect, which occurs during the clutch disengagement for gearshifting, provides the clutch actuator system with an assistant torque for fast disengagement.

VI. CONCLUSION

A novel design for a clutch actuator system was presented based upon self-energizing effect. The new clutch actuator has rack and pinion mechanism for generating reinforcement torque, and eliminates a diaphragm spring compared with conventional systems. These characteristics allow the smaller electromechanical actuator to be used and make the system more controllable.

While it is advantageous to achieve a reduced torque requirement, control performance may be deteriorated in the case of

self-locking. To solve this problem, the passivity analysis of the system is performed to derive the releasable-locking condition during clutch engagement. With this, a sliding-mode control algorithm is developed to track the desired actuator position for clutch engagement and disengagement operations in the presence of modeling uncertainties. The conceptual design of proposed system is implemented on a laboratory test bench. With the guaranteed boundness of torque amplification, the clutch position is controlled for synchronizing both sides of the clutch.

In future works, the actuation part composed of the slot joint and the worm shaft should be simplified to achieve a precise motion control. The development of a contact transition control strategy taking into account of self-energizing effect will be invaluable compared with the deterministic control strategy based on the clutch positioning.

APPENDIX A

KINEMATIC ANALYSIS

The subscript “bs” and “ws” in the variables denote the ball screw and the worm shaft, respectively. The motor angular position θ_m is converted into the linear motion x_{bs} by the ball screw and the lever as follows:

$$x_{bs} = \frac{l_{bs}}{2\pi}\theta_m \quad (36)$$

$$x_{ws} = \frac{l_1}{l_2}x_{bs}. \quad (37)$$

The variables l_{bs} , x_{bs} , l_j ($j = 1, 2$), and x_{ws} denote the lead length, the axial movement, the lever length, and the axial movement, respectively. Since the rotation of the worm shaft on the slot joint is very small, it can be expressed by

$$\theta_{ws} \approx \frac{y_{ws}}{r_{ws}} = \frac{x_{ws} \tan \alpha_{ws}}{r_{ws}} \quad (38)$$

where y_{ws} is the vertical movement, i.e., $y_{ws} = x_{ws} \tan \alpha_{ws}$, α_{ws} is the slot joint angle, r_{ws} is the radius, and θ_{ws} is the rotating angle. Since the actuation neck and the actuation plate

are connected to each other, the rotational angles of them are the same, i.e., $\theta_{ws} = \theta_a$. To eliminate the lever effect, the lever lengths are set to be equal, i.e., $l_1 = l_2$. From (36)–(38), the angular position of the actuation plate θ_a can be written as the function of motor position θ_m

$$\theta_a = \frac{l_{bs} \tan \alpha_{ws}}{2\pi r_{ws}} \theta_m. \quad (39)$$

Consequently, the equivalent conversion ratio N_g in (9) is defined as follows:

$$N_g \triangleq \frac{2\pi r_{ws}}{l_{bs} \tan \alpha_{ws}}. \quad (40)$$

APPENDIX B

SYSTEM PARAMETERS

Name	Symbol	Unit
DC Motor		
Moment of inertia	J_m	kgm^2
Torque constant	k_t	Nm/A
Viscous friction coefficient	b_m	Nms/rad
Armature inductance	L_m	H
Armature resistance	R_m	Ω
Worm Screw		
Ball-screw lead	l_{bs}	mm
Worm shaft angle	α_{ws}	deg
Worm shaft radius	r_{ws}	mm
Equivalent conversion ratio	N_g	—
Breakaway friction torque	T_{fs}	Nm
Positive Coulomb friction torque	T_{fc+}	Nm
Negative Coulomb friction torque	T_{fc-}	Nm
Actuator viscous friction torque	b_a	Nms/rad
Mechanical Actuator		
Actuator groove angle	α_{ws}	deg
Pinion gear position radius	r_p	mm
Actuation plate moment of inertia	J_a	kgm^2
Actuation plate stiffness	k_a	Nm/rad

REFERENCES

- [1] L. Petit, C. Prella, E. Dore, F. Lamarque, and M. Bigerelle, "A four-discrete-position electromagnetic actuator: Modeling and experimentation," *IEEE/ASME Trans. Mechatronics*, vol. 15, no. 1, pp. 88–96, Feb. 2010.
- [2] L. Yan, I.-M. Chen, C. K. Lim, G. Yang, W. Lin, and K.-M. Lee, "Design and analysis of a permanent magnet spherical actuator," *IEEE/ASME Trans. Mechatronics*, vol. 13, no. 2, pp. 239–248, Apr. 2008.
- [3] B.-S. Kim, J.-B. Song, and J.-J. Park, "A serial-type dual actuator unit with planetary gear train: Basic design and applications," *IEEE/ASME Trans. Mechatronics*, vol. 15, no. 1, pp. 108–116, Feb. 2010.
- [4] Y. Zhang, G. Liu, and J. Hesselbach, "On development of a rotary to linear actuator using piezoelectric translators," *IEEE/ASME Trans. Mechatronics*, vol. 11, no. 5, pp. 647–650, Oct. 2006.
- [5] H.-S. Yan and Y.-C. Wu, "A novel design of a brushless dc motor integrated with an embedded planetary gear train," *IEEE/ASME Trans. Mechatronics*, vol. 11, no. 5, pp. 551–557, Oct. 2006.
- [6] L. Glielmo, L. Iannelli, V. Vacca, and F. Vasca, "Gearshift control for automated manual transmission," *IEEE/ASME Trans. Mechatronics*, vol. 11, no. 1, pp. 17–26, 2006.
- [7] J. Horn, J. Bambergera, P. Michaux, and S. Pindlb, "Flatness-based clutch control for automated manual transmissions," *Control Eng. Practice*, vol. 11, pp. 1353–1359, 2003.
- [8] B. Matthes, "Dual clutch transmissions—Lessons learned and future potential," SAE, Tech. Rep. 2005-01-1021, 2005.
- [9] U. Wagner and A. Wagner, "Electrical shift gearbox (esg)—Consistent development of the dual clutch transmission to a mild hybrid system," SAE, Tech. Rep. 2005-01-4182, 2005.
- [10] F. Garofalo, L. Glielmo, L. Iannelli, and F. Vasca, "Optimal tracking for automotive dry clutch engagement," presented at the IFAC 15th Triennial World Congr., Barcelona, Spain, 2002.
- [11] M. Montanari, F. Ronchi, C. Rossi, A. Tilli, and A. Tonielli, "Control and performance evaluation of a clutch servo system with hydraulic actuation," *Control Eng. Practice*, vol. 12, pp. 1369–1379, 2004.
- [12] H. E. Merritt, *Hydraulic Control Systems*. New York: Wiley, 1967.
- [13] S. E. Moon, H. S. Kim, and S. H. Hwang, "Development of automatic clutch actuator for automated manual transmissions," *Int. J. Automot. Technol.*, vol. 6, no. 5, pp. 461–466, 2005.
- [14] A. J. Turner and K. Ramsay, "Review and development of electromechanical actuators for improved transmission control and efficiency," SAE, Tech. Rep. 2004-01-1322, 2004.
- [15] J. Kim and S. B. Choi, "Self-energizing clutch actuator system: Basic concept and design," in *Proc. FISITA2010 World Automotive Congr.*, May 2010, CD-ROM, Paper FISITA2010-SC-P-23, 8 pp.
- [16] T. Welge-Luessen and C. Glocker, "Modelling and application of the self-locking phenomenon in the context of a non-discrete impact clutch," *PAMM*, vol. 5, no. 1, pp. 221–222, Dec. 2005.
- [17] G. J. Organek and D. M. Preston, "Driveline clutch with unidirectional apply ball ramp," U.S. Patent 5 810 141, Sep. 22, 1998.
- [18] P. Dolcini, "Contribution to the clutch comfort," Ph.D. dissertation, Institut National Polytechnique de Grenoble, Grenoble, France, 2007.
- [19] H. A. Rothbart, *Mechanical Design Handbook*. New York: McGraw-Hill, 1996.
- [20] J. Fox, R. Roberts, C. Baier-Welt, L. M. Ho, L. Lacraru, and B. Gombert, "Modeling and control of a single motor electronic wedge brake," SAE, Tech. Rep. 2007-01-0866, 2007.
- [21] J. A. Collins, *Mechanical Design of Machine Elements and Machines: A Failure Prevention Perspective*. New York: Wiley, 2003.
- [22] R. Juvinall and K. Marshek, *Fundamentals of Machine Component Design*. New York: Wiley, 1991.
- [23] D. Karnopp, "Computer simulation of slip-stick friction in mechanical dynamic systems," *Trans. ASME, J. Dyn. Syst., Meas., Contr.*, vol. 107, no. 1, pp. 100–103, 1985.
- [24] M. Ebrahimi and R. Whalley, "Analysis, modeling and simulation of stiffness in machine tool drives," *Comput. Ind. Eng.*, vol. 38, no. 1, pp. 93–105, 2000.
- [25] Y. Zhu and E. Barth, "Passivity-based impact and force control of a pneumatic actuator," *Trans. ASME, J. Dyn. Syst., Meas., Contr.*, vol. 130, pp. 024 501-1–024 501-7, Mar. 2008.
- [26] R. Gorbet, K. Morris, and D. Wang, "Passivity-based stability and control of hysteresis in smart actuators," *IEEE Trans. Contr. Syst. Technol.*, vol. 9, no. 1, pp. 5–16, Jan. 2001.
- [27] C. Byrnes, A. Isidori, and J. Willems, "Passivity, feedback equivalence, and the global stabilization of minimum phase nonlinear systems," *IEEE Trans. Automat. Contr.*, vol. 36, no. 11, pp. 1228–1240, Nov. 1991.
- [28] H. Khalil, *Nonlinear System*, 3rd ed. Upper Saddle River, NJ: Prentice-Hall, 2002.
- [29] J. J. E. Slotine and W. Li, *Applied Nonlinear Control*. Englewood Cliffs, NJ: Prentice-Hall, 1991.
- [30] F. Vasca, L. Iannelli, A. Senatore, and M. Scafati, "Modeling torque transmissibility for automotive dry clutch engagement," in *Proc. 2008 Amer. Control Conf.*, Seattle, Washington, 2008, pp. 306–311.
- [31] V. Utkin, J. Guldner, and J. Shi, *Sliding Mode Control in Electromechanical Systems*. New York: Taylor and Francis, 1999.
- [32] K. Ohnishi, N. Matsui, and Y. Hori, "Estimation, identification, and sensorless control in motion control system," *Proc. IEEE*, vol. 82, no. 8, pp. 1253–1265, Aug. 1994.
- [33] K. Ohnishi, M. Shibata, and T. Murakami, "Motion control for advanced mechatronics," *IEEE/ASME Trans. Mechatronics*, vol. 1, no. 1, pp. 56–67, Mar. 1996.
- [34] J. Slotine and S. Sastry, "Tracking control of non-linear systems using sliding surfaces, with application to robot manipulators," *Int. J. Control*, vol. 38, no. 2, pp. 465–492, 1983.
- [35] J. Slotine, "Sliding controller design for non-linear systems," *Int. J. Control*, vol. 40, no. 2, pp. 421–434, 1984.
- [36] L. Ljung, *System Identification: Theory for the User*. Prentice Hall information and system sciences series. Englewood Cliffs, NJ: Prentice Hall, 1987.

- [37] S. Seshagiri and H. Khalil, "On introducing integral action in sliding mode control," in *Proc. 41st IEEE Conf. Decision Control*, Dec. 2002, vol. 2, pp. 1473–1478.



Jinsung Kim (S'10) received the B.S. degree in mechanical engineering from Kookmin University, Seoul, Korea, in 2007, and the M.S. degree in mechanical engineering from Korea Advanced Institute of Science and Technology, Daejeon, Korea, where he is currently working toward the Ph.D. degree in mechanical engineering.

His current research interests include automotive systems, nonlinear control, and integrated design and control of complex mechanical systems.



Seibum B. Choi (M'09) received the B.S. degree in mechanical engineering from Seoul National University, Seoul, Korea, the M.S. degree in mechanical engineering from Korea Advanced Institute of Science and Technology (KAIST), Daejeon, Korea, and the Ph.D. degree in controls from the University of California, Berkeley, in 1993.

From 1993 to 1997, he was involved in the development of automated vehicle control systems at the Institute of Transportation Studies, University of California, Berkeley. During 2006, he was with TRW, Warren, MI, where he was engaged in the development of advanced vehicle control systems. Since 2006, he has been with the faculty of the Mechanical Engineering Department, KAIST. His current research interests include fuel-saving technology, vehicle dynamics and control, and active safety systems.